MiR-21 Regulates Metabolic Adaptation of T_H17 Cells during Autoimmunity and Host Defence

Authors

Xiang Yu[1, *], Li Wang[1, *], Chao Yao[2], Rong Qiu[2], Yange Cui[2], Dai Dai[3], Jun Deng[3], Guojun Hou[2], Yan Wang[2], Jie Qian[1], Ye Ouyang[1], Yuting Qin[3], Bo Qu[1], Haibo Zhou[3], Youcun Qian[2], Yuanjia Tang[1], Nan Shen[1,2,3,4]

Affiliations

[1] Shanghai Institute of Rheumatology, Renji Hospital, Shanghai Jiao Tong University School of Medicine, Shanghai, China.
[2] Institute of Health Sciences, Shanghai Jiao Tong University School of Medicine and Shanghai Institutes for Biological Sciences (SIBS), University of Chinese Academy of Sciences, Chinese Academy of Sciences (CAS), Shanghai, China.
[3] China-Australia Centre for Personalized Immunology, Renji Hospital, Shanghai Jiao Tong University School of Medicine, Shanghai, China.
[4] Center for Autoimmune Genomics and Etiology (CAGE), Cincinnati Children's Hospital Medical Center, Cincinnati, Ohio, USA.
Correspondence to Nan Shen, MD, Department of Rheumatology, Renji Hospital, Shanghai Jiao Tong University School of Medicine, 145 Shan Dong Road (c), Shanghai 200001, China. E-mail: nanshensibs@gmail.com.
* These authors contributed equally.

Summary

T_H17 cells exhibit great heterogeneity and variable functional states in vivo. However, metabolic adaptation of T_H17 cells in vivo and its regulation during autoimmunity and host defence is unknown. Here we report that T_H17 cells derived in vivo under homeostatic or autoimmune condition show discrete metabolic states. Metabolic states of T_H17 cells in vivo were controlled at the epigenetic level, with conserved regulatory region of key metabolic genes show

distinct chromatin accessibility as demonstrated by global chromatin landscape profiling. Mechanistically key regulatory region of a group of microRNAs were shown to be with increased chromatin openness under autoimmune condition, and *miR-21* was identified as an essential metabolic regulator of T_H17 cells. Understanding the regulation of T_H17 cell metabolic adaptation in vivo may therefore provide more defined therapeutic intervention to T_H17 cell mediated autoimmune diseases and insights into T_H17 cell mediated host defence.

Keywords

T_H17 cell, metabolic adaptation, chromatin states, autoimmune disease, mucosal immunity

Introduction

T_H17 cells, which have been characterized as a subset of effector $CD4^+$ helper T cells that produce IL-17A(Littman and Rudensky, 2010). Under steady state condition, T_H17 cells producing IL-10 are mainly found at sites of intestinal lamina propria, where they mediate mucosal defense(Ivanov et al., 2009; Sano et al., 2015). Under autoimmune and pathogen infection condition, T_H17 cells acquire the capability to produce IFNγ or GM-CSF, and are often seen at sites of inflamed loci(Atarashi et al., 2015; Stockinger and Omenetti, 2017). T_H17 cells also could be differentiated in vitro by a combination of cytokines TGF-β1, IL-6 or IL-6, IL-1β and IL-23(Ghoreschi et al., 2010).

Studies have shown that T_H17 cells can selectively produce IL-10 or IFNγ when mice are infected with different pathogens, and IL-1R signaling is essential for

the induction of IFNγ while suppressing of IL-10(Zielinski et al., 2012). The cytokine GM-CSF also is reported to be critical for the pathogenesis of T_H17 cells(Codarri et al., 2011; El-Behi et al., 2011). Recently it is reported that environmental factors such as salt can function to promote pathogenic T_H17 cells development in vivo. Sodium chloride induced Sgk1 is essential for the maintenance of T_H17 cells(Kleinewietfeld et al., 2013; Wu et al., 2013). And by single cell RNA-seq of both in vitro and in vivo-derived T_H17 cells, CD5L was identified as a potential negative regulator of the pathogenicity of T_H17 cells(Gaublomme et al., 2015; Wang et al., 2015).

Upon antigen stimulation, lymphocytes undergo extensive clonal expansion and differentiation for immune defense and regulation(Boothby and Rickert, 2017; Buck et al., 2015; Man and Kallies, 2015; Pollizzi and Powell, 2014). Activated lymphocytes are highly metabolic and demonstrate a striking increase in cell size and glycolysis acitivity. c-Myc, Hif1a, c-Rel and mTORc1-dependent glycolytic activity is crucial for effective T and B cell immune response(Shi et al., 2011; Verbist et al., 2016; Wang et al., 2011), whereas Foxo1 and Foxp3 proteins function as key metabolic repressors that contain glycolytic activity in Treg cells(Angelin et al., 2017; Wilhelm et al., 2016). Recently it is reported that by restricting glucose availability, tumor cells limit aerobic glycolysis and effector function of tumor-infiltrating T cells(Chang et al., 2015; Ho et al., 2015). So far, the metabolic states of T_H17 cells in vivo under different circumstances is unknown, and how T_H17 cells adapt to different

microenvironment with distinct nutrition supply were not known.

MicroRNAs are a class of noncoding RNAs that modulate gene expression at the posttranscriptional level(Mehta and Baltimore, 2016). Specific microRNAs, such as *miR-146a* and *miR-155*, were initially shown to be upregulated during macrophage inflammatory response. Mice deficient of *miR-146a* had severe multiple organ autoimmune disease(Boldin et al., 2011). And *miR-155*$^{-/-}$ mice had reduced germinal center response under viral infection(Rodriguez et al., 2007; Thai et al., 2007); however, these mice were highly resistant to develop EAE disease due to defective T_H17 cell differentiation(Escobar et al., 2014; O'Connell et al., 2010). Recently, *miR-183-96-182* cluster was also reported to be critical for T_H17 cell pathogenicity(Ichiyama et al., 2016). However, the regulation of T_H17 cell metabolic adaptation in vivo to distinct microenvironment by microRNAs is not well understood.

Recently, Assay for transposase-accessible chromatin (ATAC-seq) technology was developed to study global chromatin changes by using relatively low cell number(Buenrostro et al., 2013). It was successfully used to study global chromatin dynamics of Treg cells under inflammatory condition(van der Veeken et al., 2016), the development of plasmacytoid DC (Ceribelli et al., 2016)and tumor-specific $CD8^+$ T cells(Philip et al., 2017).

In this study, first by metabolomics study we found in vitro derived T_H17 cells under non-pathogenic and pathogenic condition had distinct metabolic states.

Further by RNA-seq of T_H17 cells derived in vivo under homeostatic and autoimmune condition, we demonstrate that T_H17 cells adapt to microenvironment with discrete metabolic states. And the metabolic states of T_H17 cells in vivo was regulated at the epigenetic level as revealed by globally chromatin landscape profiling. Mechanistically we found key regulatory region of *miR-21* was with enhanced chromatin accessibility under autoimmune and pathogen infection condition, we further demonstrate that miR-21 is essential for the metabolic function of T_H17 cells, and miR-21-regulated metabolic adaptation of T_H17 cells is required for autoimmune disease progression and mucosal defence. These findings suggest that miR-21 is a critical regulator for the metabolic adaptation of T_H17 cells during autoimmunity and mucosal defence.

Results

T_H17 Cells show discrete metabolic states in vitro

To study the metabolic activity of T_H17 cells, first we induced T_H17 cells in vitro by a combination of cytokines TGF-β1, IL-6 (T_H17 (b)) or IL-6, IL-1β and IL-23 (T_H17 (23)). Interestingly, we consistently observed that T_H17 (23) cells show increased cell size compared to T_H17 (b) cells (Figure S1A-B), which indicate that T_H17 (23) cells are more metabolically activated. We further tested the metabolic potential of T_H17 (b) and T_H17 (23) cells by analyzing key metabolic regulators and enzymes, we found p-S6 and HKII were immediately activated during T_H17 cell differentiation, and T_H17 (23) cells were much more glycolytic

than T_H17 (b) cells, T_H17 (23) cells express great more p-S6, HKII at the protein level (Figure 1A). To study early metabolic requirements needed for T_H17 cell differentiation, we checked key metabolic activator and repressor at an earlier time point, 30h after initial activation, we found T_H17 (23) cells express great more HKII, Glut1, p-S6 and c-Myc, while express lower level of the metabolic repressor protein Foxo1 (Figure 1B-C). To study the metabolic potential of T_H17 cells more clearly, we sorted GFP^+ T_H17 cells differentiated in vitro from IL17A-eGFP mice, again we found T_H17 (23) cells express great more HKII, the rate limiting enzyme for glycolysis (Figure 1D).

We further subjected T_H17 (b) and T_H17 (23) cells for high-resolution metabolomics analyses. Pathogenic T_H17 (23) cells were metabolically distinct from T_H17 (b) cells (Figure 1E, Figure S1C), and showed higher level intermediates of carbohydrates, amino acids and organic acids, while T_H17 (b) cells showed higher level intermediates of nucleotides and fatty acids. Pathway analyses of altered metabolites showed that amino acid, amino sugar metabolism, and glycolytic intermediates trended higher in T_H17 (23) cells (Figure 1F, Table S1). Taken together, these data suggest that T_H17 cells differentiated in vitro under non-pathogenic and pathogenic condition have distinct metabolic states.

T_H17 Cells show discrete metabolic states in vivo

To gain insight of the metabolic adaptation of T_H17 cells in vivo, we first immunized IL17A-eGFP mice with MOG_{35-55} emulsified in complete adjuvant to

induce autoimmune EAE, and infected IL17A-eGFP mice with enteric pathogen *Citrobacter Rodentium* to induce colitis. Then we analyzed and sorted GFP$^+$ T_H17 cells from homeostatic ileum, CNS of EAE mice at the peak of disease and *Citrobacter*-infected colon tissue (Figure S2A). Interestingly after gating on T_H17 cells, we found CNS-infiltrated and *Citrobacter*-induced T_H17 cells had significantly increased cell size compared to ileum homeostatic T_H17 cells (Figure 2A), which indicate T_H17 cells derived under autoimmune and pathogen infection condition are more metabolically activated. To gain a more global view of functional and metabolic states of T_H17 cells in vivo, we sent ileum homeostatic and CNS-infiltrated T_H17 cells for RNA-seq analyses. We found 1415 upregulated genes and 1249 downregulated genes in CNS-infiltrated T_H17 cells compared to ileum homeostatic T_H17 cells. GO and Pathway analyses indicate that several immune pathways were activated in CNS-infiltrated T_H17 cells as reported, interestingly, we found multiple metabolic pathways were enriched (Figure 2B), of the 1415 upregulated genes, almost 10% were involved in metabolic process, which indicate T_H17 cells adapt to diverse microenvironment with discrete metabolic states. We found homeostatic T_H17 cells express great more *c-Kit* (Figure 2C), which is critical for maintenance of quiescent hematopoietic stem cells, suggest it would play a similar role here by keep the quiescence of ileum homeostatic T_H17 cells. Ileum homeostatic T_H17 cells also express several transcription factors with repressor activity, *Foxp1*, *c-Maf* and *Foxo1*, and Foxo1 was a repressor of glucose

metabolism(Wilhelm et al., 2016) (Figure 2C), which is consistent with our finding that CNS-infiltrated T_H17 cells express higher level genes of the glucose metabolism pathway (Figure 2D). Further analyses of the data revealed that of the 66 differentially expressed solute carrier family genes, almost 70% were upregulated in CNS-infiltrated T_H17 cells (Figure 2E), which indicate that T_H17 cells in vivo adapt to microenvironment with distinct pattern of solute carrier proteins for different nutrition needs. Taken together, these data suggest that T_H17 cells in vivo adapt to microenvironment with discrete metabolic states to facilitate their inflammatory or regulatory function.

Epigenetic regulation of T_H17 Cell metabolic adaptation in vivo

To dissect the possible regulation mechanism for T_H17 cell adaptation in vivo, we performed ATAC-seq to assess chromatin landscape genome-wide of T_H17 cells derived in vivo. We found that T_H17 cells had discrete chromatin states in vivo (Figure 3A-B). CNS infiltrating T_H17 cells showed great differential global chromatin accessibility compared to ileum homeostatic T_H17 cells, whereas the difference between colon *Citro Rodentium* induced T_H17 cells and ileum homeostatic T_H17 cells was much smaller. Principle component analysis of enriched peaks indicated that T_H17 cells in vivo had discrete chromatin states (Figure 3C), with the major variance came from CNS infiltrating T_H17 cells, chromatin states between ileum homeostatic and *Citro Rodentium* induced colon T_H17 cells were much similar, which indicate these two types of T_H17 cells may have similar functional property, for mucosal defense against intestinal

pathogens. Interestingly, the regulatory region of key T_H17 cell-related transcription factors c-*Maf* and *Ahr* was with reduced chromatin accessibility in CNS infiltrating T_H17 cells, both c-Maf and Ahr were shown to be critical regulators of T_H17 cells, whereas the regulatory region of metabolic repressor Foxo1 was with reduced chromatin accessibility in CNS-infiltrated T_H17 cells, which suggests that CNS-infiltrated T_H17 cells were relieved from Foxo1-mediated metabolic repression (Figure 3D). A group of genes related to metabolic pathways and solute carrier family members were also with enhanced chromatin accessibility in CNS-infiltrated T_H17 cells, which was consistent with the gene expression data (Figure 3D, Figure S3). Together, these data suggest metabolic states of T_H17 cells in vivo were consistent with their epigenetic states and therefore were regulated at the epigenetic level.

Genomic region of microRNAs shows discrete chromatin accessibility

Interestingly, we found that the regulatory region of certain microRNAs showed great more chromatin accessibility in CNS infiltrating T_H17 cells compared to ileum homeostatic T_H17 cells, which include *miR-21, miR-23a cluster,* and *miR-210* (Figure 4A-B). The regulatory region of *miR-125a* cluster was with reduced chromatin accessibility in CNS infiltrating T_H17 cells, which indicate that this microRNA cluster might have some regulatory role in intestinal homeostatic T_H17 cells, as reported for its regulatory role in regulatory T cells(Pan et al., 2015). The regulatory region of *miR-155, miR-146, miR-17-92 cluster* and *miR-183-96-182* cluster was with the same chromatin accessibility between T_H17

cells derived at different conditions in vivo (Figure 4A-B), many of them were already shown to be critical for effector CD4$^+$ T cell and Treg cell function. These data suggest that microRNAs may regulate the metabolic adaptation of T_H17 cells in vivo under autoimmune and pathogen infection condition.

Our group previously demonstrated that miR-21 was highly upregulated in inflammatory lesions of multiple human autoimmune diseases(Zhu et al., 2012). A deep-sequencing survey of the miRNome in mouse CD4$^+$ helper T cell subsets derived in vitro showed high level of miR-21 in inflammatory T_H17 cells(Ichiyama et al., 2016), and miR-21 expression accounted for almost 20% of total microRNA counts in T_H17 cells (Figure S4A-B). To better understand the regulation of metabolic adaptation in vivo by small microRNAs, we focused on miR-21 for further study. We activated naive CD4$^+$ T cells in the presence of anti-CD3 and anti-CD28 with or without IL-6, IL-23, IL-1β or TGF-β1. Among the cytokines tested, IL-6 appeared to be a critical factor for miR-21 upregulation (Figure S4C). IL-1β and IL-23 could further promote IL-6-induced miR-21 expression. IL-6 promotes T_H17 cell differentiation by activating Stat3, which directly drives the transcription of T_H17 lineage-specific genes, including *Rorc*, *Il17* and *Il23r*. We further validated these results by using *Stat3* conditional knockout mice in CD4$^+$ T cells (Figure S4D). These data suggest that IL-6-STAT3 signaling is essential for miR-21 upregulation in inflammatory T_H17 cells.

MiR-21 is critical for the development of homeostatic T_H17 cells in vivo

We further studied the role of miR-21 in T_H17 cells by *miR-21*$^{-/-}$ mice. And we found normal T cell development and homeostasis in *miR-21*$^{-/-}$ mice. Then, we tested whether miR-21 was essential for naïve CD4$^+$ T cell activation and T_H17 cell differentiation in vitro. When activated with anti-CD3 and anti-CD28, CFSE-labeled *miR-21*$^{-/-}$ CD4$^+$ T cells proliferated normally just as control CD4$^+$ T cells, which indicated that miR-21 was not essential for initial activation-induced proliferation of CD4$^+$ T cells (Figure S5A). Loss of miR-21 did not impact T_H17 cell differentiation induced by TGF-β1 and IL-6 (Figure S5B). It was reported that T_H17 cells could be induced by a combination of three inflammatory cytokines that is IL-6, IL-1β and IL-23, without exogenous TGF-β1. Interestingly, under this pathogenic T_H17 polarization condition, *miR-21*$^{-/-}$ CD4$^+$ T cells were less efficiently differentiated into T_H17 cells (Figure S5B-D). These results indicate that miR-21 is required for the differentiation of T_H17 cells under IL-6/IL-1β/IL-23 condition.

At steady state, intestinal lamina propria provides a unique environment for the differentiation of T_H17 cells. IL-10 producing intestinal lamina propria T_H17 cells mediate mucosal defense and barrier tissue integrity. To investigate the role of miR-21 in T_H17 cells under a more physiological condition, we checked the presence of intestinal lamina propria T_H17 cells in control and *miR-21*$^{-/-}$ mice (Figure 5A). We found that *miR-21*$^{-/-}$ mice have significantly reduced percentage of ileum RORc$^+$ FoxP3$^-$ T_H17 cells and RORc$^+$ Tregs in vivo. We further checked the presence of intestinal lamina propria T_H17 cells in control

and CD4-cre *miR-21*$^{f/f}$ mice (Figure 5B, Figure S5E), we found that CD4-cre *miR-21*$^{f/f}$ mice have significantly reduced percentage of ileum RORc^{+} FoxP3^{-} T_H17 cells and RORc^{+} Tregs in vivo, which suggest that T cell expression of miR-21 is critical for the development of T_H17 cells under homeostatic condition.

MiR-21 regulates metabolic function of T_H17 cells through Peli1-c-Rel axis

To better understand the general functional features of miR-21-deficient T_H17 cells, we differentiated naïve T cells from control and *miR-21*$^{-/-}$ mice in vitro under pathogenic T_H17-skewing condition, RNA was extracted and subjected to RNA-seq to profile gene expression. We then analyzed the gene list for enrichment of gene ontology and canonical pathways using the DAVID bioinformatics databases(Huang da et al., 2009). In the absence of miR-21, T_H17 cells showed decreased expression of T_H17 cell signature genes, which include lineage-specific transcription factors, cytokines, and cytokine receptors (Figure 6A). Remarkably, many of the genes involved in glycolytic or related metabolic pathways were highly enriched, include key transporters for glucose intake, *Slc2a1/3*, and rate-limiting enzymes, *Hk1/2*, *Pfkl*, *Pgm2*, *Ldha* and *Pdk1* (Figure 6A, Figure S6A). We further checked the glycolytic activity of control and *miR-21*$^{-/-}$ T_H17 cells by glycolysis stress test for extracellular acidification rate, both basal and maximal glycolytic capability were greatly decreased in *miR-21*$^{-/-}$ T_H17 cells compared to control T_H17 cells (Figure 6B). By sorting out GFP^{+} control and *miR-21*$^{-/-}$ T_H17 cells differentiated from IL17A-eGFP mice, we

found T_H17 (23) cells had higher p-S6 protein level compared to T_H17 (b) cells (Figure 6C). However, *miR-21*$^{-/-}$ T_H17 (23) cells show lower p-S6 protein level compared to control T_H17 (23) cells, which indicates that miR-21 is indeed critical for the metabolic function of T_H17 cells.

To further investigate the precise mechanism underlying how miR-21 promotes T_H17 cell commitment and its metabolic function, we screened the direct targets of miR-21 by combining target prediction with Ago2 HITS-CLIP(Loeb et al., 2012), TargetScan and RNA-seq data to identify overlapping gene transcripts. Using a combination of these three approaches, we identified 5 common putative targets (*Esyt2, Mbnl1, Pdcd4, Peli1,* and *Psrc1*) (Figure 6D). Among them, Peli1 has been reported to function as a negative regulator of CD4+ T cell activation by ubiquitination of c-Rel and *Peli1*$^{-/-}$ mice spontaneously developed autoimmune disease(Chang et al., 2011). c-Rel was reported to be a metabolic regulator of germinal center B cell function(Heise et al., 2014), and was critical for T_H17 cell differentiation(Ruan et al., 2011), therefore we chose Peli1 for further analysis (Figure 6D). By in vitro RNA immunoprecipitation assay, we found Ago2-immunoprecipitated RNAs had significantly reduced Peli1 mRNA level in *miR-21*$^{-/-}$ T_H17 (23) cells (Figure 6E-F), which suggests that Peli1 is a functional target of miR-21 in T_H17 cells. We further validated these at the protein level in purified GFP$^+$ T_H17 cells differentiated in vitro, we found that *miR-21*$^{-/-}$ T_H17 cells have elevated level of Peli1 protein, whereas the protein level of c-Rel was reduced in *miR-21*$^{-/-}$ T_H17 cells (Fig. 6G). Interestingly,

we found that T_H17 (23) cells expressed substantially high level of c-Rel compared to T_H17 (b) cells, and TGFβ1 signaling is required for the repression of c-Rel expression (Figure S6B-C). Taken together, these data suggest that miR-21 targets the Peli1-c-Rel pathway to promote the metabolic and effector function of T_H17 cells.

MiR-21 regulates T_H17 cells during autoimmunity and mucosal defence

To determine the role of miR-21 in a T_H17 cell dominant disease model, we performed passive EAE to specifically address the role of miR-21 in mediating CNS inflammation induced by pre-activated $MOG_{35–55}$-specific T_H17 cells (Figure S7A-C). When adoptively transferred into naive recipient mice, only control MOG-specific T_H17 cells efficiently induced EAE (Figure S7D), *miR-21*$^{-/-}$ T_H17 cells failed to induce EAE, emphasizing an indispensable role of miR-21 in mediating the cell-intrinsic effector function of T_H17 cells.

To exclude any possible role of miR-21 in dendritic cells and other myeloid cells that could contribute to EAE disease pathogenesis, we bred *miR-21*$^{f/+}$ allele to CD11c-cre and Lyz-cre, to delete miR-21 in dendritic cells, neutrophils, macrophages and microglia (Figure. S7E-F). Loss of miR-21 expression in dendritic cell and myeloid cell compartment did not protect mice from autoantigen challenge (Figure 7A). When immunized with MOG_{35-55} in CFA, CD4-cre *miR-21*$^{f/f}$ mice were highly resistant to EAE compared to littermate CD4-cre mice (Figure 7B-E). At the peak of disease, CD4-cre *miR-21*$^{f/f}$ mice had less infiltrating of $CD4^+$ IL-$17A^+$ $IFN\gamma^+$ and $IL17A^+$ GM-CSF^+ T_H17 cells.

To explore miR-21 mediated T_H17 cell function in an enteric pathogen infection condition, we used *Citrobacter Rodentium*-induced colitis, mice-deficient of Il17A gene exhibit much severe colitis and bacteria clearance(Basu et al., 2015). After gavage control and CD4-cre *miR-21*$^{f/f}$ mice with *Citrobacter*, we found that CD4-cre *miR-21*$^{f/f}$ mice suffered from more severe colitis, with significantly shorter colon and increased luminal bacteria load by day 14 compared to control mice (Figure 7F-G). Further analyses of colon lamina propria lymphocytes revealed that infected CD4-cre *miR-21*$^{f/f}$ mice had significantly lower number of total $CD4^+$ T cells, T_H17 and T_H1 cells, albeit with the same number of T_H17*1 cells (Figure 7H-K). Taken together, these data demonstrate that miR-21 mediates autoimmune disease and mucosal defence through T_H17 cells in a $CD4^+$ T cell intrinsic manner.

Discussion

T_H17 cells exhibit great heterogeneity in vivo, the basic energy requirement of T_H17 cells for their regulatory or inflammatory function under homeostatic or autoimmune and pathogen infection condition was not examined. And how T_H17 cells adapt to diverse tissue microenvironment with distinct nutrition availability and regulation of their metabolic adaptation in vivo were not known. In the present study, by metabolomics analyses of in vitro derived T_H17 cells, we found that T_H17 cells respond to different stimulations with distinct metabolic activity. And by global transcriptome analyses of in vivo derived T_H17 cells, we first showed T_H17 cells adapt to tissue microenvironment with discrete

metabolic states in vivo.

To dissect the regulation of T_H17 cell metabolic states in vivo, we performed genome-wide chromatin landscape analysis and found that T_H17 cells had discrete chromatin states in vivo. The regulatory region of key T_H17 cell-related transcription factors, metabolic regulators, metabolism-related genes and microRNAs were with differential chromatin accessibility between homeostatic ileum T_H17 cells and CNS infiltrating T_H17 cells. Interestingly, colon T_H17 cells from *Citro Rodentium* infected mice had similar chromatin status with homeostatic ileum T_H17 cells, which indicates that they have similar anti-bacteria function in vivo. Our data suggests that T_H17 cells in vivo adapt to distinct microenvironment with discrete epigenetic and metabolic states, and metabolic regulators and metabolism-related genes were regulated at the epigenetic level for their functional requirements.

Interestingly, we found the conserved regulatory region of a group of small microRNAs were with differential chromatin accessibility of T_H17 cells derived in vivo, which could have contributed to the regulation of discrete metabolic states of T_H17 cells in vivo for the fine-tune property of microRNAs. In particular, the regulatory region of miR-21 was with increased chromatin accessibility in CNS infiltrating T_H17 cells. We found that T_H17 cells expressed higher amount of miR-21 (almost 20% total microRNA counts), which was dependent on IL-6-STAT3 axis.

In the current study, we demonstrate that miR-21 was essential for steady state

intestinal LP T_H17 development in vivo in a $CD4^+$ T cell intrinsic manner. Higher miR-21 expression in the inflamed CNS tissue of autoimmune EAE mice has been observed in CNS infiltrating $CD4^+$ T cells, dendritic cells and other myeloid cells. In our study, we demonstrated that miR-21 expression in $CD4^+$ T cells but not on dendritic cells were critically required for T_H17 cell mediated autoimmune disease and mucosal defence against enteric pathogen *Citrobacter*.

Although miR-21 was shown previously to be important in T_H17 cell generation(Murugaiyan et al., 2015), its exact action has not been well understood. By global transcriptomics analyses, we demonstrate that miR-$21^{-/-}$ T_H17 cells express less T_H17 cell signature genes and key metabolism pathway genes. Further by purify T_H17 cells differentiated from IL17A-eGFP mice, we found *miR-21*$^{-/-}$ T_H17 cells had reduced mTORc1 activity, with dramatically reduced intracellular p-S6 level. These data suggest that with increased chromatin openness of its regulatory region, miR-21 promotes metabolic function of T_H17 cells under autoimmune inflammation.

To survey for putative targets of miR-21 in pathogenic T_H17 cells, we combined target prediction with previously reported miR-21 Ago HITS-CLIP data, TargetScan and our RNA-seq data to identify overlapping gene transcripts. Using a combination of these three approaches, we identified Peli1 as a functional target of miR-21 in pathogenic T_H17 cells. Peli1 has been reported to function as a negative regulator of $CD4^+$ T cell activation by ubiquitination of c-Rel and *Peli1*$^{-/-}$ mice spontaneously developed autoimmune disease. To our

knowledge, our study identifies the first evidence that by targeting key downstream regulators of TCR signaling miR-21 promotes the metabolic adaptation of T_H17 cells and regulates T_H17 cell during autoimmunity and host defence.

Experimental Procedures

Mice

MiR-21$^{-/-}$ and *miR-21* $^{f/+}$ mice on the C57B6 background were from Biomodel Organism (Shanghai, China). CD4-cre, Lyz-cre, CD11c-cre and *Stat3* $^{f/+}$ mice were from Jackson lab. IL17A-eGFP reporter mice were from Biocytogen. All mice were maintained under specific pathogen-free conditions. All animal experiments were performed in compliance with the guide for the care and use of laboratory animals and were approved by the institutional biomedical research ethics committee of the Shanghai Institutes for Biological Sciences (Chinese Academy of Sciences).

Cell culture

Naïve $CD4^+$ T cells were isolated from lymph nodes or spleen of mice using a $CD4^+$ $CD62L^+$ T cell isolation kit II (Miltenyi Biotec) according to the manufacturer's instruction. Naïve $CD4^+$ T cells were stimulated with plate-bound anti-CD3ε mAb (5 μg/ml) in the presence of anti-CD28 mAb (2 μg/ml) in a 48-well plate under neutral conditions (10 μg/ml anti–IL-4 mAb and 10 μg/ml anti–IFN-γ mAb), IL-6 conditions (10 ng/ml IL-6, 10 μg/ml anti–IL-4 mAb, and

10 µg/ml anti–IFN-γ mAb), T_H17 (b) conditions (2 ng/ml TGF-β, 20 ng/ml IL-6, 10 µg/ml anti–IL-4 mAb, and 10 µg/ml anti–IFN-γ mAb), T_H17 (23) conditions (20 ng/ml IL-6, 20 ng/ml IL-1β, 20 ng/ml IL-23, 10 µg/ml anti–IL-4 mAb, and 10 µg/ml anti–IFN-γ mAb).

Antibodies and reagents

Antibodies to mouse CD3ε (145-2C11), CD28 (37.51), IL-4 (11B11), IFN-γ (XMG1.2), CD3ε PerCP5.5 (145-2C11), Foxp3 APC (FJK-16s), ROR gamma (t) PE (B2D) and GM-CSF PE (MP1-22E9) were from eBiosciences. Antibodies to mouse CD45 APC-cy7 (30-F11), CD4 BV510 (RM4-5), IL-17A PE (TC11-18H10), IFN-γ APC (XMG1.2) were from BD Biosciences. Recombinant Mouse IL-6, IL-1β, IL-23, and TGF-β1 protein were purchased from R&D Systems. Peli1 (F-7) was from Santa cruz, c-Rel (D4Y6M), Foxo1 (C29H4), p-S6 (2F9), c-Myc (D3N8F), HKII (C64G5) were from Cell signaling. Glut1 (EPR3915) antibody was from Abcam. RIPAb+ Ago2 was from Merk millipore. XF Glycolysis Stress Test Kit was from Agilent technologies.

Intracellular cytokine staining

Cultured or tissue isolated lymphocytes were washed and stimulated with PMA (50 ng/ml) plus ionomycin (750 ng/ml) for 4 h at 37°C. Cells were stained with anti-CD45 APC-cy7, anti-CD3ε PerCP5.5 and anti-CD4 BV510 for 30 min at 4°C. Cells were then fixed, permeabilized with Perm/Wash buffer (BD), and stained with anti–IFN-γ APC, anti-GM-CSF PE or anti–IL-17A PE for 30 min at

4°C. Cytokine profiles of $CD4^+$ cells were analyzed on a FACSCalibur with FlowJo software (Tree Star).

Induction of EAE

IL17A-eGFP reporter mice, $CD4^{cre}$ miR-$21^{fl/fl}$ mice and littermate CD4-cre or miR-$21^{fl/fl}$ mice were injected subcutaneously in the tail base with MOG35-55 peptide (200 μg/mouse, MEVGWYRSPFSRVVHLYRNGK) in complete Freund's adjuvant. 5 min and 48 h after the injection of MOG35-55 peptide, the mice were injected intraperitoneally with pertussis toxin (200 ng/mouse; Sigma-Aldrich). Status of the mice was monitored, and disease severity was scored three times a week as follows: 0 = no clinical signs, 1 = limp tail (tail paralysis), 2 = complete loss of tail tonicity or abnormal gait, 3 = partial hind limb paralysis, 4 = complete hind limb paralysis, 5 = forelimb paralysis or moribund, 6 = death. Cells were isolated from whole brain and spinal cord at the peak of disease by Percoll gradient centrifugation (37%/70%) and subjected to flow cytometric analysis or flow cytometric sorting.

***Citro Rodentium* infection**

C. rodentium strain DBS100 (ATCC51459; American Type Culture Collection) were prepared by shaking of bacteria overnight at 37 °C in Luria-Bertani broth. Bacterial cultures were serially diluted and plated on MacConkey agar plates so the CFU dose administered could be confirmed. For infection, IL17A-eGFP reporter mice were oral inoculated with 2×10^9 CFU C. rodentium in a total

volume of 100 ul per mouse. T_H17 cells were isolated from colon tissue by Percoll gradient centrifugation (40%/80%) and subjected to flow cytometric sorting at day 10.

RNA-seq

Naive $CD4^+$ T cells from control and *miR-21*$^{-/-}$ mice were differentiated under pathogenic T_H17 (23) differentiation condition. Total RNA was prepared from these cells using Trizol reagent (Invitrogen). RNA-seq libraries were prepared using a SureSelect Strand Specific RNA Library Preparation kit (Agilent). Sequencing was performed on an Illumina HiSeq1500 using a TruSeq Rapid SBS kit (Illumina) in a 50-base single-end mode. mRNA profiles were calculated with a Cufflinks software and expressed as FPKM (fragments per kilobase of exon model per million mapped fragments).

ATAC-seq

ATAC-seq library preparations were performed as described(Buenrostro et al., 2013). In brief, 50,000 cells were washed in cold PBS and lysed. Transposition was performed at 37 °C for 30 min. After purification of the DNA with the MinElute PCR purification kit (Qiagen), DNA was amplified for 5 cycles. Additional PCR cycles were evaluated by real time PCR. Final product was cleaned by Ampure Beads at a 1.5× ratio. Libraries were sequenced on a Hiseq 2500 1T in a 50 bp/50 bp Paired end run, using the TruSeq SBS Kit v3 (Illumina).

Metabolomics

The untargeted metabolomics profiling was performed on XploreMET platform (Metabo-Profile, Shanghai, China). MetaboAnalyst was used to analyze range-scale data and provide PCA and KEGG pathway analysis of metabolites changed (www.metaboanalyst.ca/).

Statistics

Prism software was used for statistical analysis. Differences between groups were compared with an unpaired two-tailed t-test. A P value of less than 0.05 was considered statistically significant.

Acknowledgments

We thank Youcun Qian for kindly sharing with us *C. rodentium* strain DBS100.

Author Contributions

X.Y. and N.S. designed the experiments and wrote the manuscript; X.Y. did most of the experiments; L.W. helped with the mouse experiments; C.Y. and R. Q. helped with the ATAC-seq data analysis; Y.C. helped with cell culture.

Declaration of Interests

The authors declare no competing financial interests.

References

Angelin, A., Gil-de-Gomez, L., Dahiya, S., Jiao, J., Guo, L., Levine, M.H., Wang, Z., Quinn, W.J., 3rd, Kopinski, P.K., Wang, L., et al. (2017). Foxp3 Reprograms T Cell Metabolism to Function in Low-Glucose, High-Lactate Environments. Cell metabolism.

Atarashi, K., Tanoue, T., Ando, M., Kamada, N., Nagano, Y., Narushima, S., Suda, W., Imaoka, A., Setoyama, H., Nagamori, T., et al. (2015). Th17 Cell Induction by Adhesion of Microbes to Intestinal Epithelial Cells. Cell *163*, 367-380.

Basu, R., Whitley, S.K., Bhaumik, S., Zindl, C.L., Schoeb, T.R., Benveniste, E.N., Pear, W.S., Hatton, R.D., and Weaver, C.T. (2015). IL-1 signaling modulates activation of STAT transcription factors to antagonize retinoic acid signaling and control the TH17 cell-iTreg cell balance. Nature immunology *16*, 286-295.

Boldin, M.P., Taganov, K.D., Rao, D.S., Yang, L., Zhao, J.L., Kalwani, M., Garcia-Flores, Y., Luong, M., Devrekanli, A., Xu, J., et al. (2011). miR-146a is a significant brake on autoimmunity, myeloproliferation, and cancer in mice. The Journal of experimental medicine *208*, 1189-1201.

Boothby, M., and Rickert, R.C. (2017). Metabolic Regulation of the Immune Humoral Response. Immunity *46*, 743-755.

Buck, M.D., O'Sullivan, D., and Pearce, E.L. (2015). T cell metabolism drives immunity. The Journal of experimental medicine *212*, 1345-1360.

Buenrostro, J.D., Giresi, P.G., Zaba, L.C., Chang, H.Y., and Greenleaf, W.J. (2013). Transposition of native chromatin for fast and sensitive epigenomic profiling of open chromatin, DNA-binding proteins and nucleosome position. Nature methods *10*, 1213-1218.

Ceribelli, M., Hou, Z.E., Kelly, P.N., Huang, D.W., Wright, G., Ganapathi, K., Evbuomwan, M.O., Pittaluga, S., Shaffer, A.L., Marcucci, G., et al. (2016). A Druggable TCF4- and BRD4-Dependent Transcriptional Network Sustains Malignancy in Blastic Plasmacytoid Dendritic Cell Neoplasm. Cancer cell *30*, 764-778.

Chang, C.H., Qiu, J., O'Sullivan, D., Buck, M.D., Noguchi, T., Curtis, J.D., Chen, Q., Gindin, M., Gubin, M.M., van der Windt, G.J., et al. (2015). Metabolic Competition in the Tumor Microenvironment Is a Driver of Cancer Progression. Cell *162*, 1229-1241.

Chang, M., Jin, W., Chang, J.H., Xiao, Y., Brittain, G.C., Yu, J., Zhou, X., Wang, Y.H., Cheng, X., Li, P., et al. (2011). The ubiquitin ligase Peli1 negatively regulates T cell activation and prevents autoimmunity. Nature immunology *12*, 1002-1009.

Codarri, L., Gyulveszi, G., Tosevski, V., Hesske, L., Fontana, A., Magnenat, L., Suter, T., and Becher, B. (2011). RORgammat drives production of the cytokine GM-CSF in helper T cells, which is essential for the effector phase of autoimmune neuroinflammation. Nature immunology *12*, 560-567.

El-Behi, M., Ciric, B., Dai, H., Yan, Y., Cullimore, M., Safavi, F., Zhang, G.X., Dittel, B.N., and Rostami, A. (2011). The encephalitogenicity of T(H)17 cells is dependent on IL-1- and IL-23-induced production of the cytokine GM-CSF. Nature immunology *12*, 568-575.

Escobar, T.M., Kanellopoulou, C., Kugler, D.G., Kilaru, G., Nguyen, C.K., Nagarajan, V., Bhairavabhotla, R.K., Northrup, D., Zahr, R., Burr, P., et al. (2014). miR-155 activates cytokine gene expression in Th17 cells by regulating the DNA-binding protein Jarid2 to relieve polycomb-mediated repression. Immunity *40*, 865-879.

Gaublomme, J.T., Yosef, N., Lee, Y., Gertner, R.S., Yang, L.V., Wu, C., Pandolfi, P.P., Mak, T., Satija, R., Shalek, A.K., et al. (2015). Single-Cell Genomics Unveils Critical Regulators of Th17 Cell Pathogenicity. Cell *163*, 1400-1412.

Ghoreschi, K., Laurence, A., Yang, X.P., Tato, C.M., McGeachy, M.J., Konkel, J.E., Ramos, H.L., Wei, L., Davidson, T.S., Bouladoux, N., et al. (2010). Generation of pathogenic T(H)17 cells in the absence of TGF-beta signalling. Nature *467*, 967-971.

Heise, N., De Silva, N.S., Silva, K., Carette, A., Simonetti, G., Pasparakis, M., and Klein, U. (2014). Germinal center B cell maintenance and differentiation are controlled by distinct NF-kappaB transcription factor subunits. The Journal of experimental medicine *211*, 2103-2118.

Ho, P.C., Bihuniak, J.D., Macintyre, A.N., Staron, M., Liu, X., Amezquita, R., Tsui, Y.C., Cui, G., Micevic, G., Perales, J.C., et al. (2015). Phosphoenolpyruvate Is a Metabolic Checkpoint of Anti-tumor T Cell Responses. Cell *162*, 1217-1228.

Huang da, W., Sherman, B.T., and Lempicki, R.A. (2009). Systematic and integrative analysis of large gene lists using DAVID bioinformatics resources. Nature protocols *4*, 44-57.

Ichiyama, K., Gonzalez-Martin, A., Kim, B.S., Jin, H.Y., Jin, W., Xu, W., Sabouri-Ghomi, M., Xu, S., Zheng, P., Xiao, C., et al. (2016). The MicroRNA-183-96-182 Cluster Promotes T Helper 17 Cell Pathogenicity by Negatively Regulating Transcription Factor Foxo1 Expression. Immunity *44*, 1284-1298.

Ivanov, II, Atarashi, K., Manel, N., Brodie, E.L., Shima, T., Karaoz, U., Wei, D., Goldfarb, K.C., Santee, C.A., Lynch, S.V., et al. (2009). Induction of intestinal Th17 cells by segmented filamentous bacteria. Cell *139*, 485-498.

Kleinewietfeld, M., Manzel, A., Titze, J., Kvakan, H., Yosef, N., Linker, R.A., Muller, D.N., and Hafler, D.A. (2013). Sodium chloride drives autoimmune disease by the induction of pathogenic TH17 cells. Nature *496*, 518-522.

Littman, D.R., and Rudensky, A.Y. (2010). Th17 and regulatory T cells in mediating and restraining inflammation. Cell *140*, 845-858.

Loeb, G.B., Khan, A.A., Canner, D., Hiatt, J.B., Shendure, J., Darnell, R.B., Leslie, C.S., and Rudensky, A.Y. (2012). Transcriptome-wide miR-155 binding map reveals widespread noncanonical microRNA targeting. Molecular cell *48*, 760-770.

Man, K., and Kallies, A. (2015). Synchronizing transcriptional control of T cell metabolism and function. Nature reviews. Immunology *15*, 574-584.

Mehta, A., and Baltimore, D. (2016). MicroRNAs as regulatory elements in immune system logic. Nature reviews. Immunology *16*, 279-294.

Murugaiyan, G., da Cunha, A.P., Ajay, A.K., Joller, N., Garo, L.P., Kumaradevan, S., Yosef, N., Vaidya, V.S., and Weiner, H.L. (2015). MicroRNA-21 promotes Th17 differentiation and mediates experimental autoimmune encephalomyelitis. The Journal of clinical investigation *125*, 1069-1080.

O'Connell, R.M., Kahn, D., Gibson, W.S., Round, J.L., Scholz, R.L., Chaudhuri, A.A., Kahn, M.E., Rao, D.S., and Baltimore, D. (2010). MicroRNA-155 promotes autoimmune inflammation by enhancing inflammatory T cell development. Immunity *33*, 607-619.

Pan, W., Zhu, S., Dai, D., Liu, Z., Li, D., Li, B., Gagliani, N., Zheng, Y., Tang, Y., Weirauch, M.T., et al. (2015). MiR-125a targets effector programs to stabilize Treg-mediated immune homeostasis. Nature communications *6*, 7096.

Philip, M., Fairchild, L., Sun, L., Horste, E.L., Camara, S., Shakiba, M., Scott, A.C., Viale, A., Lauer, P., Merghoub, T., et al. (2017). Chromatin states define tumour-specific T cell dysfunction and

reprogramming. Nature *545*, 452-456.

Pollizzi, K.N., and Powell, J.D. (2014). Integrating canonical and metabolic signalling programmes in the regulation of T cell responses. Nature reviews. Immunology *14*, 435-446.

Rodriguez, A., Vigorito, E., Clare, S., Warren, M.V., Couttet, P., Soond, D.R., van Dongen, S., Grocock, R.J., Das, P.P., Miska, E.A., et al. (2007). Requirement of bic/microRNA-155 for normal immune function. Science (New York, N.Y.) *316*, 608-611.

Ruan, Q., Kameswaran, V., Zhang, Y., Zheng, S., Sun, J., Wang, J., DeVirgiliis, J., Liou, H.C., Beg, A.A., and Chen, Y.H. (2011). The Th17 immune response is controlled by the Rel-RORgamma-RORgamma T transcriptional axis. The Journal of experimental medicine *208*, 2321-2333.

Sano, T., Huang, W., Hall, J.A., Yang, Y., Chen, A., Gavzy, S.J., Lee, J.Y., Ziel, J.W., Miraldi, E.R., Domingos, A.I., et al. (2015). An IL-23R/IL-22 Circuit Regulates Epithelial Serum Amyloid A to Promote Local Effector Th17 Responses. Cell *163*, 381-393.

Shi, L.Z., Wang, R., Huang, G., Vogel, P., Neale, G., Green, D.R., and Chi, H. (2011). HIF1alpha-dependent glycolytic pathway orchestrates a metabolic checkpoint for the differentiation of TH17 and Treg cells. The Journal of experimental medicine *208*, 1367-1376.

Stockinger, B., and Omenetti, S. (2017). The dichotomous nature of T helper 17 cells. Nature reviews. Immunology.

Thai, T.H., Calado, D.P., Casola, S., Ansel, K.M., Xiao, C., Xue, Y., Murphy, A., Frendewey, D., Valenzuela, D., Kutok, J.L., et al. (2007). Regulation of the germinal center response by microRNA-155. Science (New York, N.Y.) *316*, 604-608.

van der Veeken, J., Gonzalez, A.J., Cho, H., Arvey, A., Hemmers, S., Leslie, C.S., and Rudensky, A.Y. (2016). Memory of Inflammation in Regulatory T Cells. Cell *166*, 977-990.

Verbist, K.C., Guy, C.S., Milasta, S., Liedmann, S., Kaminski, M.M., Wang, R., and Green, D.R. (2016). Metabolic maintenance of cell asymmetry following division in activated T lymphocytes. Nature *532*, 389-393.

Wang, C., Yosef, N., Gaublomme, J., Wu, C., Lee, Y., Clish, C.B., Kaminski, J., Xiao, S., Meyer Zu Horste, G., Pawlak, M., et al. (2015). CD5L/AIM Regulates Lipid Biosynthesis and Restrains Th17 Cell Pathogenicity. Cell *163*, 1413-1427.

Wang, R., Dillon, C.P., Shi, L.Z., Milasta, S., Carter, R., Finkelstein, D., McCormick, L.L., Fitzgerald, P., Chi, H., Munger, J., et al. (2011). The transcription factor Myc controls metabolic reprogramming upon T lymphocyte activation. Immunity *35*, 871-882.

Wilhelm, K., Happel, K., Eelen, G., Schoors, S., Oellerich, M.F., Lim, R., Zimmermann, B., Aspalter, I.M., Franco, C.A., Boettger, T., et al. (2016). FOXO1 couples metabolic activity and growth state in the vascular endothelium. Nature *529*, 216-220.

Wu, C., Yosef, N., Thalhamer, T., Zhu, C., Xiao, S., Kishi, Y., Regev, A., and Kuchroo, V.K. (2013). Induction of pathogenic TH17 cells by inducible salt-sensing kinase SGK1. Nature *496*, 513-517.

Zhu, S., Pan, W., Song, X., Liu, Y., Shao, X., Tang, Y., Liang, D., He, D., Wang, H., Liu, W., et al. (2012). The microRNA miR-23b suppresses IL-17-associated autoimmune inflammation by targeting TAB2, TAB3 and IKK-alpha. Nature medicine *18*, 1077-1086.

Zielinski, C.E., Mele, F., Aschenbrenner, D., Jarrossay, D., Ronchi, F., Gattorno, M., Monticelli, S., Lanzavecchia, A., and Sallusto, F. (2012). Pathogen-induced human TH17 cells produce IFN-gamma or IL-10 and are regulated by IL-1beta. Nature *484*, 514-518.

Figure Legends

Figure 1 T_H17 Cells show discrete metabolic states in vitro

(A) Western blot analysis of HKII and p-S6 in total protein from $CD4^+$ T cells activated in vitro for indicated time, T_H17 (b) and T_H17 (23) cells differentiated in vitro for 72 h.

(B) Western blot analysis of Foxo1, c-Myc and p-S6 in total protein from T_H17 (b) and T_H17 (23) cells differentiated in vitro for indicated time.

(C) Western blot analysis of HKII and Glut1 in total protein from T_H17 (b) and T_H17 (23) cells differentiated in vitro for indicated time.

(D) Western blot analysis of HKII in total protein from purified GFP^+ T_H17 (b) and T_H17 (23) cells differentiated in vitro for 72 h.

(E) PCA analysis of identified metabolites of T_H17 (b) and T_H17 (23) cells differentiated in vitro for 48 hs by metabolomics.

(F) Metabolomics analysis of T_H17 (b) and T_H17 (23) cells differentiated in vitro for 48 hs, the top differentially observed metabolites are shown in heat map. Data are from one experiment representative of two independent experiments (A, B), >3 independent experiments (C, D).

Figure 2 T_H17 Cells show discrete metabolic states in vivo

(A) Forward scatter plot of T_H17 cells derived in vivo

(B) Side scatter plot of T_H17 cells derived in vivo

(C) Pathway analysis of upregulated genes in CNS T_H17 cells, presented as enrichment for selected pathways.

(D) Heat map of selected genes of interest in T_H17 cell biology.

(E) Heat map of upregulated genes in CNS T_H17 cells related to metabolism pathways.

(F) Heat map of differentially expressed solute carrier family genes.

Figure 3 Epigenetic regulation of T_H17 Cell metabolic adaptation in vivo

(A) Scatterplots of mean ATAC-seq counts per peak comparing the indicated samples.

(B) Scatterplots of mean ATAC-seq counts per peak comparing the indicated samples.

(C) Principal component analysis (PCA) of peak accessibility in ileum (blue), colon *Citrobacter* (yellow) and CNS (red) T_H17 cells.

(D) ATAC-seq signal profiles across *Ahr*, *c-Maf*, *Foxo1, Pfkfb3* and *Hk3* gene loci.

Figure 4 Genomic region of microRNAs shows discrete chromatin accessibility

(A) ATAC-seq signal profiles across *miR-155, miR-146a, miR-17-92* cluster and *miR-182* cluster gene loci.

(B) ATAC-seq signal profiles across *miR-21, miR-23a* cluster*, miR-210* and *miR-125a* cluster gene loci.

Figure 5 MiR-21 is critical for the development of homeostatic T_H17 cells in vivo

(A) Flow cytometry of $CD4^+$ T cells from 7-week old naïve control and *miR-21*$^{-/-}$ mice (n=3) ileum lamina propria, numbers in quadrants indicate percent cells in each.

(B) Flow cytometry of $CD4^+$ T cells from 7-week old naïve CD4-cre and CD4-cre *miR-21*$^{f/f}$ mice (n=3) ileum lamina propria, numbers in quadrants indicate percent cells in each.

(C) Percentage of $RORc^+$ $FOXP3^-$ T_H17 cells, $RORc^+$ $FOXP3^+$ and $RORc^-$ $FOXP3^+$ Treg cells from ileum lamia propria of control and *miR-21*$^{-/-}$ mice as in (A).

(D) Percentage of $RORc^+$ $FOXP3^-$ T_H17 cells, $RORc^+$ $FOXP3^+$ and $RORc^-$ $FOXP3^+$ Treg cells from ileum lamia propria of CD4-cre and CD4-cre *miR-21*$^{f/f}$ mice as in (B).

Figure 6 MiR-21 regulates metabolic function of T_H17 cells through Peli1-c-Rel axis

(A) Heat map of selected genes of interest in T_H17 cell pathogenicity (left) and in glycolytic pathways (right).

(B) Extracellular acidification rate (ECAR) of T_H17 (23) cells differentiated from control and *miR-21*$^{-/-}$ mice for 96 hs assessed by a glycolysis stress test.

(C) Western blot analysis of p-S6 from sorted GFP$^+$ T_H17 cells differentiated under indicated condition.

(D) Comparison of gene list from RNA-seq, Targetscan and CLIP-seq data, showing an overlap of 5 potential miR-21 target genes.

(E) RT-PCR analysis of enriched Peli1 mRNA from Ago2 immunoprecipitated total RNA from in vitro differentiated Control and *miR-21*$^{-/-}$ T_H17(23) cells.

(F) The 3' UTR of Peli1 in activated CD4$^+$ T cells from HITS-CLIP data.

(G) Western blot analysis of Peli1 and c-Rel from sorted GFP$^+$ T_H17 cells differentiated under indicated condition.

Figure 7 MiR-21 regulates T_H17 cells during autoimmunity and mucosal defence

(A) EAE development in CD4-cre and CD4-cre *miR-21*$^{f/f}$ (n=5) mice.

(B) EAE development in Lyz2-cre and Lyz2-cre *miR-21*$^{f/f}$ (n=7) mice.

(C) EAE development in CD11c-cre and CD11c-cre *miR-21*$^{f/f}$ (n=7) mice.

(D) Flow cytometry of IL-17A and IFN-γ secretion by $CD4^+$ T cells isolated from spinal cord of CD4-cre and CD4-cre *miR-21*$^{f/f}$ mice at the peak of disease (n = 4).

(E) Percentage of $IL17A^+$ IFN-γ^-, $IL17A^+$ IFN-γ^+ and $IL17A^-$ IFN-γ^+ cells from spinal cord of CD4-cre and CD4-cre *miR-21*$^{f/f}$ mice as in (D).

(F) Colon length of CD4-cre and CD4-cre *miR-21*$^{f/f}$ mice infected with *Citro Rodentium* for 14 days.

(G) Quantification of bacterial burden in colon luminal content at day 14.

(H) Number of total $CD4^+$ T cells of CD4-cre and CD4-cre *miR-21*$^{f/f}$ mice infected with *Citro Rodentium* for 14 days.

(I) Number of total T_H1 cells of CD4-cre and CD4-cre *miR-21*$^{f/f}$ mice infected with *Citro Rodentium* for 14 days.

(J) Number of total T_H17 cells of CD4-cre and CD4-cre *miR-21*$^{f/f}$ mice infected with *Citro Rodentium* for 14 days.

(K) Number of total T_H17*1 cells of CD4-cre and CD4-cre *miR-21*$^{f/f}$ mice infected with *Citro Rodentium* for 14 days.

Figure 1

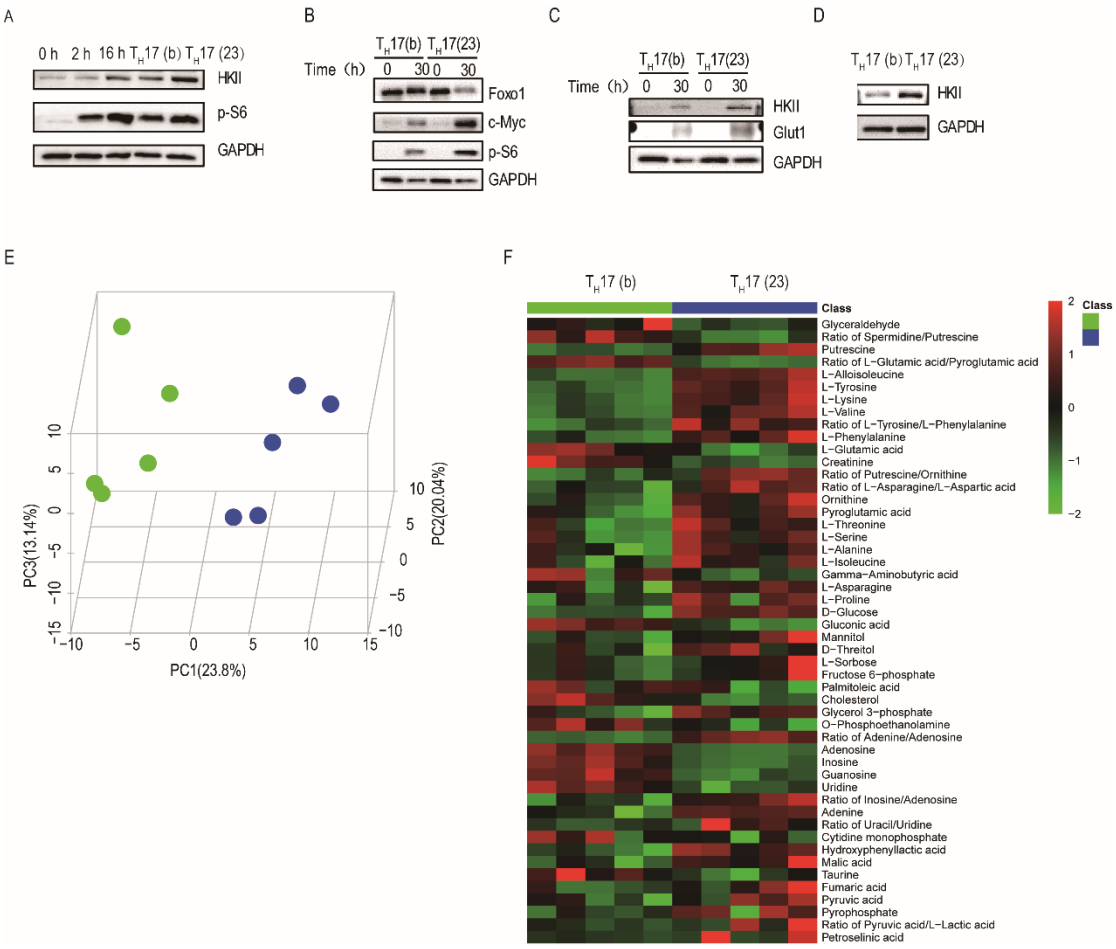

Figure 2

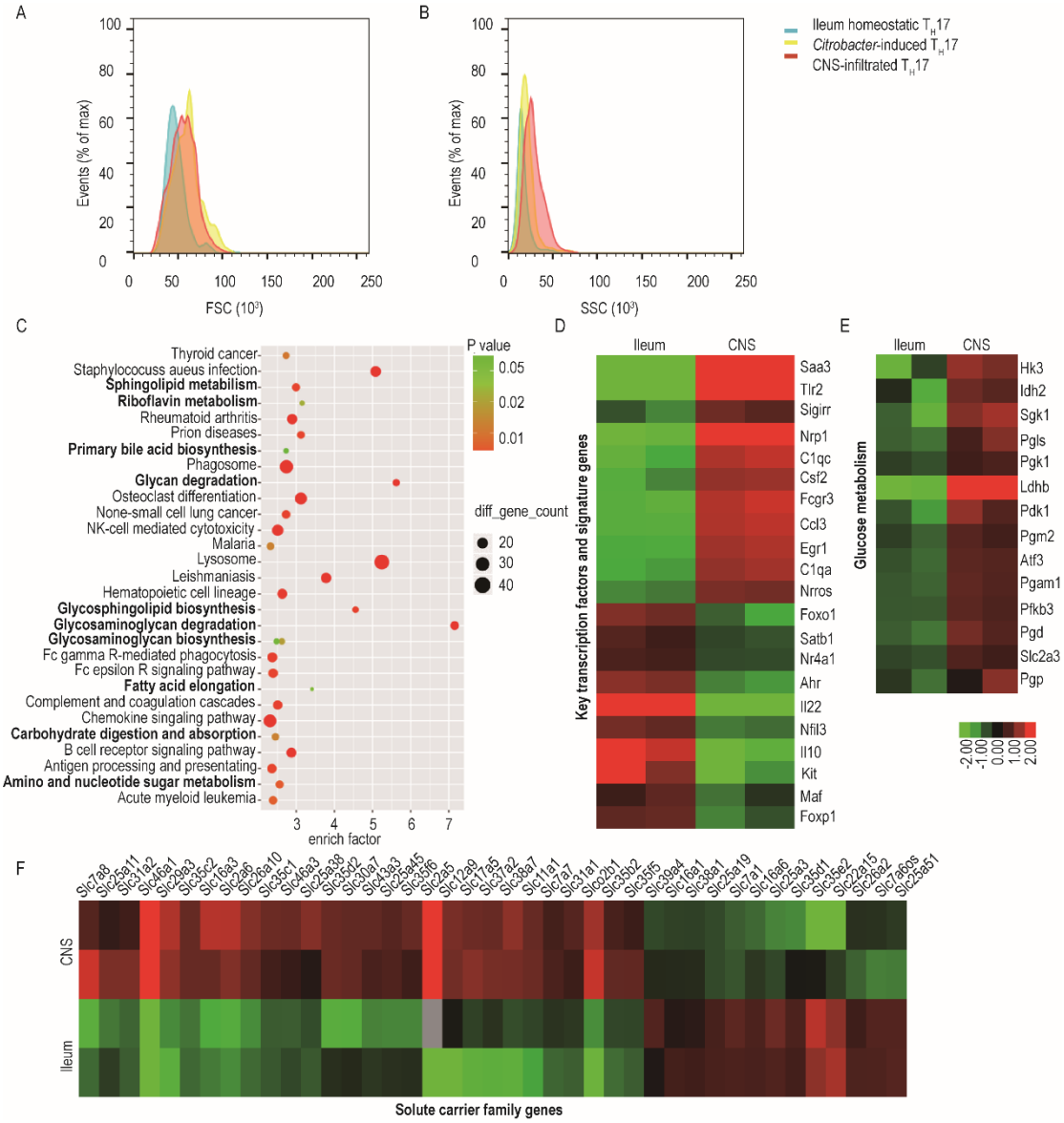

Figure 3

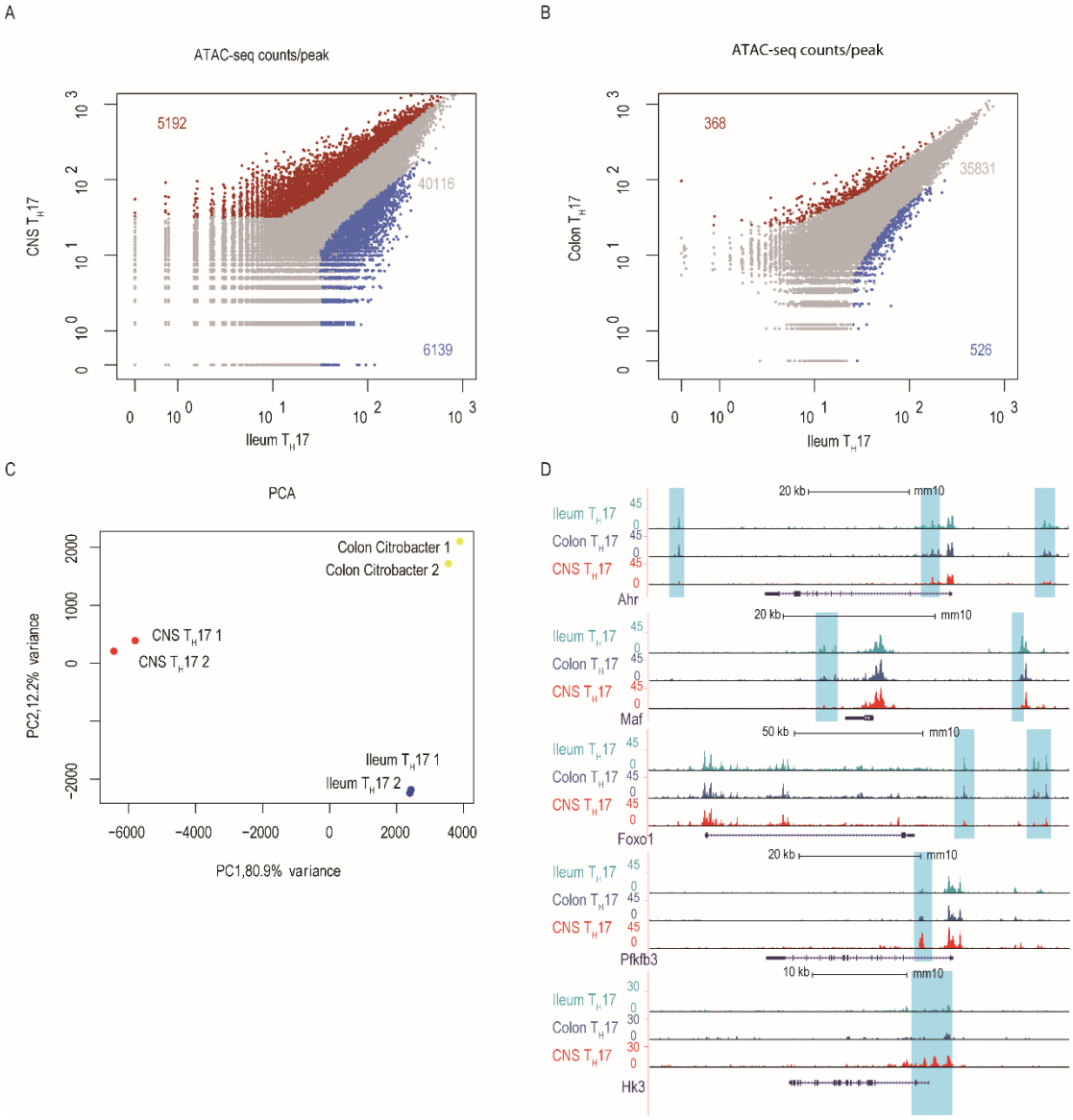

Figure 4

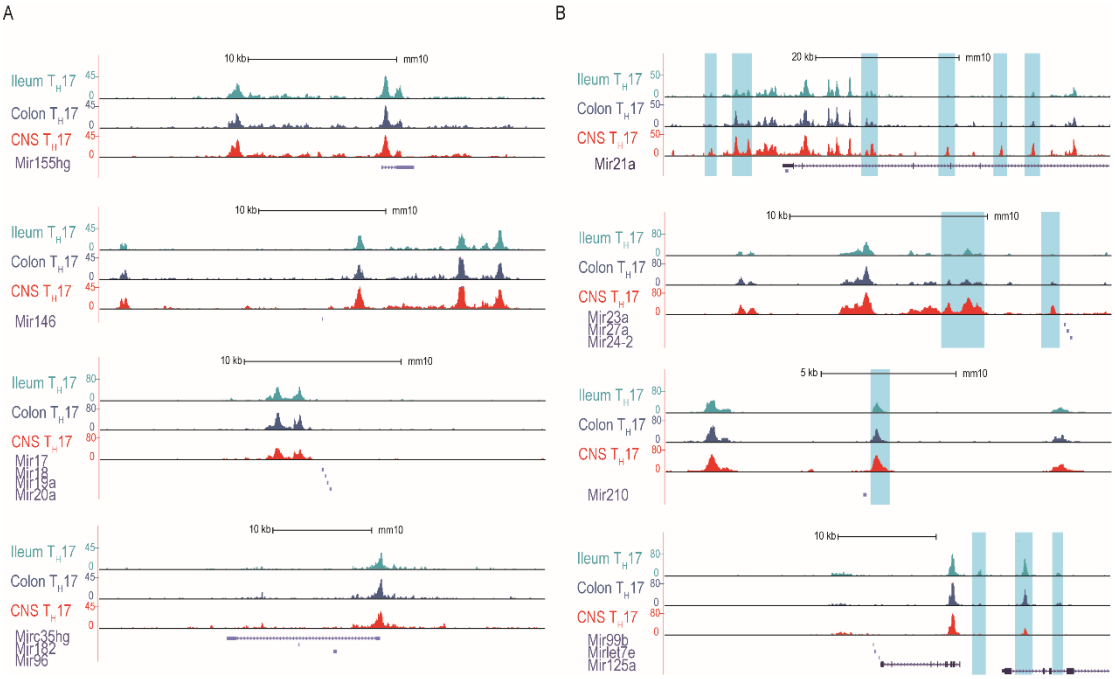

Figure 5

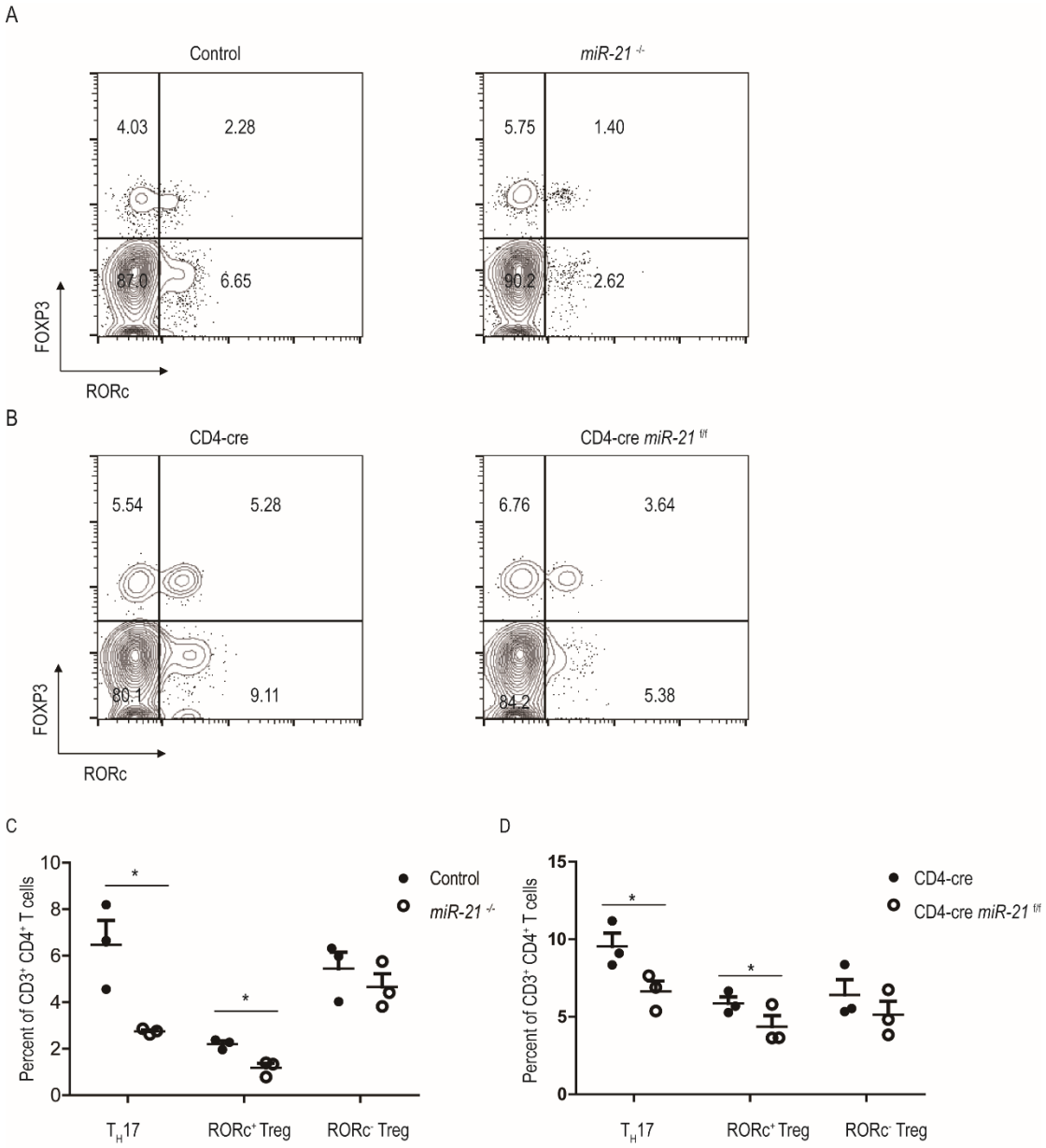

Figure 6

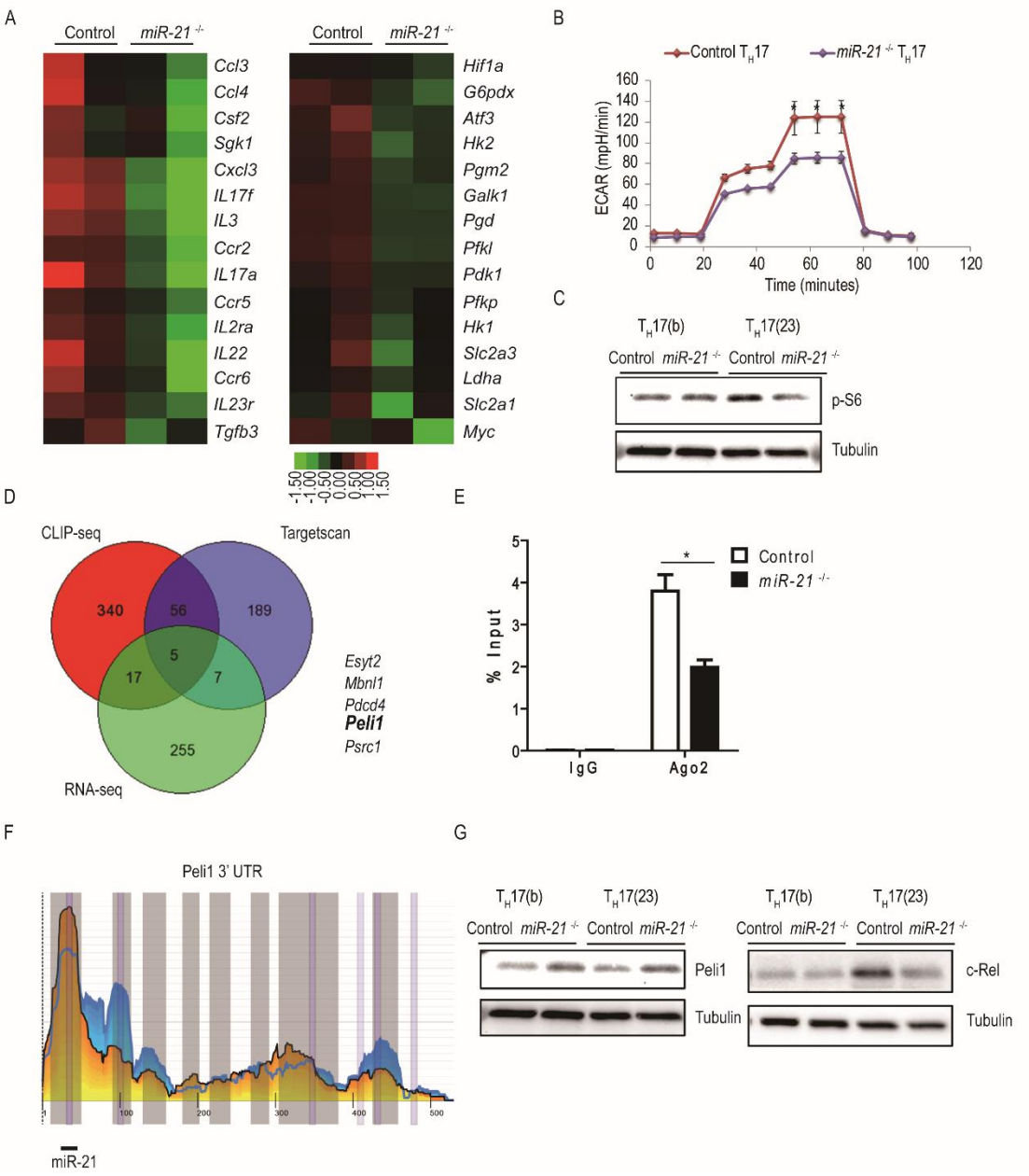

Figure 7